

Design of hot-rolled CHS steel members by advanced inelastic analysis with CSM strain limits

Miriam Corsinovi

*Department of Civil and Environmental Engineering
Imperial College London*

Abstract

Traditional steel frame design usually involves a structural analysis (i.e. first or second order elastic analysis) to determine design forces and moments. Subsequently, the members stability is assessed through individual member checks and a cross-section classification establishes the deformation capacity of the cross-sections. Beam finite element (FE) models are widely used for structural design because they are computationally efficient. However, their limitation is that they cannot capture local buckling. For this reason, an advanced inelastic analysis using beam FE models with the continuous strength method (CSM) has been developed for the design of steel structures (Fieber, Gardner & Macorini, 2020). To capture cross-section failure, the analysis requires the use of the CSM strain limits, which are applied along a characteristic length of the steel member to consider the beneficial effects from the local moment gradients. The present research carries out a second order inelastic analysis on hot-rolled circular hollow sections (CHS) steel members. The proposed design method is validated against the benchmark shell finite element models, which are deemed able to accurately capture the local buckling. Comparisons against the EN 1993-1-1(2005) design provisions are undertaken to demonstrate the advantage of using second order inelastic analysis in terms of the ultimate capacity. The proposed method has already been conducted on structural steel and stainless steel I-section and rectangular section members (Fieber, Gardner & Macorini, 2019a; Walport, Gardner & Nethercot, 2021). This research aims to fulfil the equivalent analysis on CHS members subjected to uniform bending and three-point bending. For the latter a thorough assessment is conducted to evaluate the most appropriate critical strain averaging length along the member.

1. Introduction

Circular Hollow Sections (CHS) have been used in a wide range of structural systems since the 1800s. Tubular shapes for a cross-section enable the design of the structures to be functional, but also aesthetically appealing. Because of their excellent properties, the application field is very broad: from buildings and walls where the CHS are used, to bridges in the case of arches and braces. Many offshore structures, towers and masts are designed with CHS members because their closed shape prevents the extension of corrosion and allows the structure to resist in most severe environments (Wardenier, 2002). The manufacturing of this type of cross-sections is mostly divided in two methods for the case of structural steel: the hot-rolling and cold-forming. Respectively, the sectional properties and dimensions are standardised by the BS

4848-2 (1991) and the BS 6363 (1983). The aim of the present paper is to design structural steel CHS members using second order inelastic analysis to capture instability effects such as local buckling, plasticity, local geometric imperfections and residual stresses. Beam finite elements are typically used to model structural steel beams because of their computational efficiency. Nevertheless, they cannot capture local buckling and, therefore, the design would lead to overestimate the cross-section capacities. Conversely, the shell FE models can capture the local instabilities, however they are more computational demanding than beam finite elements. For this reason, shell FE models are used as a benchmark to evaluate the validity of the proposed beam FE design method. With the purpose of simulating local buckling on the beam FE models and taking account of the local cross-section deformation, the proposed method involves the use of the strain limits with the continuous strength method (CSM) (Gardner, 2008). Thereby, the spread of plasticity and the strain hardening through the cross-sections can be controlled and the decreasing stiffness of the members due to buckling and plasticity will be modelled (Fieber, Gardner & Macorini, 2019a). Therefore, the advanced inelastic analysis permits to bypass the individual member and cross-sections checks proposed in the EN 1993-1-1 (2005) and instead it allows to design all cross-sections in the same agreeing approach. In the current paper the proposed method is applied to hot-rolled steel members with CHS subjected to uniform bending and three-point bending test. The accuracy of the analysis is checked against the benchmark shell FE models. Some comparisons are undertaken against the Eurocode provisions to demonstrate their conservativity in term of ultimate moment capacity.

2. Current Eurocode provisions

Current Eurocode design methods for CHS in EN 1993-1-1 (2005) require the cross-section classification where each class corresponds to an idealised response as illustrated in Figure 1. It permits plastic analyses only for stocky cross-sections (class 1), disregarding the strain

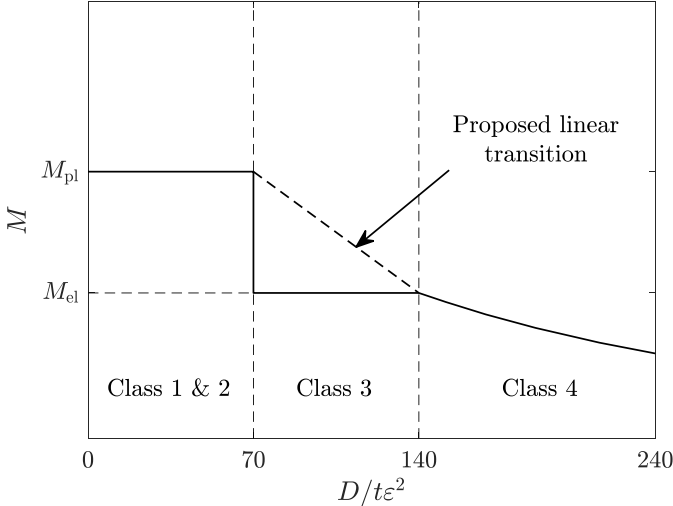


Figure 1. Current EC3 design curve and proposed design curve for pure bending

hardening and limiting the maximum stress to the yield strength f_y . In the case of higher classes, an elastic analysis is necessary because of the occurring of local buckling that does not permit the development of plastic hinges. In EN 1993-1-1 (2005), for members subjected to pure bending, class 1 cross-sections can form plastic hinges and fully reach their plastic moment resistance M_{pl} . Class 2 cross-sections behave similarly, but their rotation capacity is limited due to the triggering of the local buckling. Class 3 cross-sections can only withstand their elastic moment resistance M_{el} because the local buckling prevents them from reaching the plastic moment resistance. Lastly,

class 4 cross-sections reach only an effective moment resistance M_{eff} . In the end, because of the dismissing of the strain hardening, the cross-sections classification leads to very conservative design provisions. Moreover, due to a high shape factor which is given by the ratio between the plastic section modulus W_{pl} and the elastic section modulus W_{el} , the sharp drop in the resistance function underestimates the capacity of class 3 cross-sections. Accordingly, a

linear transition within class 3 has also been suggested and investigated for the design of semi-compact CHS by Meng et al. (2020) as it was already been conducted for I-sections and box sections (Taras, Greiner & Unterweger, 2013). Furthermore, class 3 slender limit equal to $D/t\varepsilon^2 = 90$ (where D is the outer diameter, t the thickness, $\varepsilon = \sqrt{235/f_y}$ and f_y the material yield strength) which is present in the current version of the EN 1993-1-1 (2005) for all loading conditions, will be updated in the next revision (European Committee for Standardisation, 2018) to a value of 140 for the case of bending. The new class 3 slender limit will take account of the results found by Chan and Gardner (2008). With the aim of overcoming all the shortcomings of the traditional design approaches, an advanced inelastic analysis has been established, as presented in the current paper.

3. Benchmark shell finite element modelling

In this section the shell finite element (FE) models of CHS steel members are introduced. They will be subsequently used to assess the reliability and accuracy of the proposed design method using beam finite elements presented in the next section. The model assumptions are introduced herein, and the results obtained using the software FE Abaqus (ABAQUS, 2014) will be eventually used in comparison with the results from the proposed advanced inelastic analysis.

3.1 Modelling assumptions

The benchmark shell finite element models can directly capture the local buckling and they allow to consider local and global imperfections together with geometrical and material non-linearities. However, they are also computationally demanding. A shell finite element model has been established and then validated against previous test data by Meng et al. (2020). A lot of experimental investigations have been collected by Meng et al. (2020) to validate the shell FE models, as some laboratory testing by Sherman (1974; 1976) for the three-point bending tests of hot-rolled CHS to mention a few. Moreover, the member buckling tests have also been investigated to assess the validity of the Shell FE model (Meng et al., 2020). Geometrically and materially non-linear analyses, also including imperfections (GMNIA) have been performed to simulate the structural response of a circular hollow section member. The static Riks method is used in the FE software Abaqus within the simulation (ABAQUS, 2014). The element type adopted to create the model is a four-node doubly curved shell element with reduced integration and finite membrane strains S4R which is generally used in a wide range of analyses, especially for thin-walled structural members (ABAQUS, 2014; Meng et al., 2020). A quarter of the model has been established considering two planes of symmetry (mid-length plane and the plane perpendicular to the axis of the applied load) as shown in Figure 2. The boundary conditions of a simply supported beam have been applied to a reference point located at the end support of the beam and the six DOFs at the end section have been coupled to the reference point using the kinematic coupling. A non-uniform mesh density has been adopted. The mesh size is chosen to precisely capture local buckling. A finer mesh has been considered at the mid-span of the beam with an element size equal to $0.2\sqrt{Dt}$ where D is the outer diameter and t is the thickness of the cross-section and a coarser mesh with an element size equal to $0.6\sqrt{Dt}$ has been applied to the rest of the beam (Meng et al., 2020).

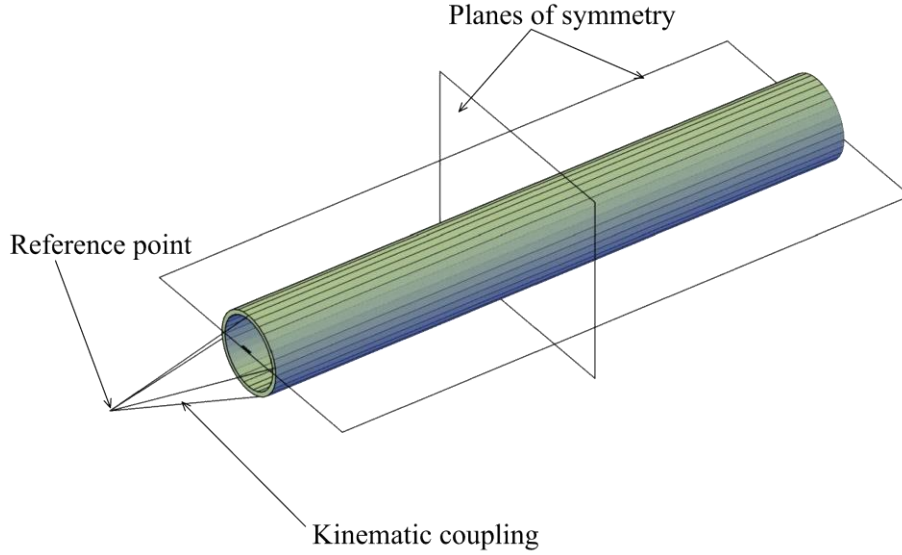


Figure 2. Quarter-model for CHS.

Initial geometric imperfections need to be included in the FE model because they have an impact on the occurring of the buckling, the spreading of plasticity and, more generally, on the ultimate capacity of the structural members. Therefore, local imperfection patterns are introduced conducting a linear bifurcation analysis (LBA) that permits to define a local buckling mode shape associated with the geometry. However, a modified thickness t_{mod} equal to $D/5$ where D is the outer diameter of the cross-section is considered to create the imperfection shape (Meng et al., 2020). The LBA has been performed with t_{mod} instead of the actual thickness because the latter revealed very short buckling half-wavelengths over the member, particularly for more slender cross-sections. Since the real local imperfection shapes exhibit longer wavelengths an LBA- t_{mod} has been found to be more realistic (Meng et al., 2020). The shape consists of a series of circumferential and meridional buckling waves and it tends to increase with the increase of the thickness because the elastic buckling wavelength of CHS is proportional to \sqrt{Dt} (Timoshenko & Woinowsky-Krieger, 1959). Typical elastic local buckling mode shapes are illustrated in Figure 3. Two cases are represented: for the three-point bending the initial imperfections are more localised at the centre of the beam, conversely for uniform bending the initial imperfections are spread along the member length. Residual stresses in both hot-rolled and cold-formed cross-sections had been investigated by Law and Gardner (2012) and by Chen and Young (2019) respectively. They demonstrated that residual stresses had a negligible influence on the cross-section behaviour for the EHS (elliptical hollow sections). For this reason, they have not been explicitly included into the shell FE model proposed for CHS (Meng & Gardner, 2020). In addition, local imperfection amplitudes have been considered equal to $0.01\sqrt{Dt}$. The length of the member is evaluated as a certain number of times the outer diameter (Meng et al., 2020). The material properties have been introduced in Abaqus (2014) in term of true stresses and logarithmic plastic strains as given by Equation (1) and (2) where E is the Young's modulus, σ_{eng} and ε_{eng} are the engineering stresses and strains respectively. It does this because the true stress-strain curve account for the changing cross-sectional area and it correctly shows the actual strain and strength of the material.

$$\sigma_{\text{true}} = \sigma_{\text{eng}}(1 + \varepsilon_{\text{eng}}) \quad (1)$$

$$\varepsilon_{\text{in}}^{\text{pl}} = \ln(1 + \varepsilon_{\text{eng}}) - \sigma_{\text{true}}/E \quad (2)$$

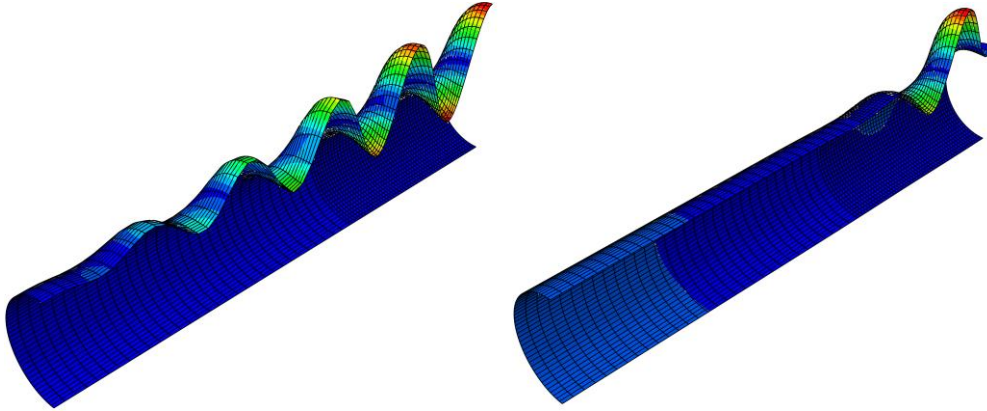


Figure 3. Elastic mode shapes for a CHS 100×3 (mm) for uniform bending (on the left) and three-point bending (on the right).

4. Second order inelastic analysis

4.1 Introduction

A method using beam finite elements with strain limits is herein introduced and successively applied in section 5. It consists in a second order inelastic analysis, where all the geometrical and material non linearities are considered (Gardner et al., 2019). It is more computationally efficient compared to the shell finite elements and, for this reason, widely used in structural design. To mimic local buckling within beam elements a continuous strength method (CSM) is used and described in the following section. It replaces the traditional cross-section classification used in EN 1993-1-1 (2005) providing a relationship between the cross-section slenderness and the strain capacity (Gardner, 2008). The CSM strain limits permit to control the plasticity redistribution within the structural members considering the local slenderness of the cross-section. Failure of steel members is assessed either if the CSM strain limit or the peak load is reached, considering the one that occurs firstly.

4.2 The continuous strength method

The continuous strength method is a deformation-based approach that consists in two fundamental components. The former is a ‘base curve’ that defines the maximum strain ϵ_{CSM} which a cross-section of a specific slenderness can withstand (Gardner, 2008). The local cross-section slenderness quantifies the level of susceptibility to local buckling and defines the strain limit in the beam finite element models. The second component considers the material non-linearity and it is a constitutive model which defines the stresses in function of the strains (Gardner et al., 2019). This approach allows to exploit the beneficial effect of the strain hardening and the spread of plasticity.

4.2.1 Base curve

The base curve defines a continuous relationship between the maximum strain ϵ_{CSM} that a cross-section can undertake before failure and the cross-section slenderness $\bar{\lambda}_c$. For the case of CHS a base curve for non-slender ($\bar{\lambda}_c \leq 0.3$) and slender ($\bar{\lambda}_c > 0.3$) cross-sections has been defined by Buchanan et al. (2016). The latter has been successively revised by Meng et al. (2019) who proposed a new base curve with a new slenderness limit $\bar{\lambda}_0 = 0.43$ (corresponding to $D/t\epsilon^2 = 200$) for the case of pure bending and $\bar{\lambda}_0 = 0.36$ (corresponding to $D/t\epsilon^2 = 140$)

for pure compression. In the present paper the base curve proposed by Meng et al. (2019) is used and the slenderness limit equal to 0.43 for pure bending is considered. The results are also compared with the ones introduced by Buchanan et al. (2016). The base curve by Meng et al. (2019) is divided in two equations and it is represented in Figure 4. For stocky cross-sections with slenderness $\bar{\lambda}_L \leq 0.43$ subjected to pure bending the strain limit is defined by the Equation (3) where B_1 represent the shape of the base curve. Two upper limits are set for the deformation capacity in Equation (3). The first one is a parameter Ω which establishes the maximum degree of plastic deformation and it is set to 15 in order to respect the material ductility requirement imposed in EN-1993-1-1 (2005). The second limit $C_1 \varepsilon_u / \varepsilon_y$ (where C_1 is a material coefficient, ε_u is the ultimate strain and ε_y is the yield strain) prevents overpredictions of the material strength. The shape factor B_1 has been calibrated using test and FE data and considering different loading conditions by Meng et al. (2019). It can be calculated by Equation (4) for the case of combined loading where Ψ is the ratio between compression and bending. Alternatively, for pure bending the shape factor B_1 is equal to 3.5 and for pure compression is equal to 2.5 (Meng et al., 2019). In the present paper the case of pure bending is investigated, therefore the CSM base curve for stocky cross-sections ($\bar{\lambda}_L < 0.43$) will be described by Equation (5). However, for slender cross-sections ($0.43 < \bar{\lambda}_L < 0.6$) failure is due to the occurring of the elastic local buckling before yielding. For the latter case, the strain limits are defined by the Winter-type design formula defined by Equation (6) where A and B_2 are coefficients which describe the shape of the design curve. B_2 is equal to 0.3 for CHS based on some calibrations (Meng et al., 2019) and A is given by Equation (7). It is important to notice that the cross-section slenderness is limited to 0.6, above this value the design of CHS refers to the shells as described in EN 1993-1-6 (2007).

$$\frac{\varepsilon_{\text{csm}}}{\varepsilon_y} = \left(\frac{\bar{\lambda}_0}{\bar{\lambda}_L} \right)^{B_1} \leq \min \left(15, \frac{C_1 \varepsilon_u}{\varepsilon_y} \right) \quad (3)$$

$$B_1 = 2.5 + \left(\frac{1 + \Psi}{2} \right)^2 \quad (4)$$

$$\frac{\varepsilon_{\text{csm}}}{\varepsilon_y} = \frac{0.121}{\bar{\lambda}_L^{2.5}} \quad \text{but} \leq \left(15, \frac{C_1 \varepsilon_u}{\varepsilon_y} \right) \quad \text{for } \bar{\lambda}_L \leq 0.43 \quad (5)$$

$$\frac{\varepsilon_{\text{csm}}}{\varepsilon_y} = \left(1 - \frac{A}{\bar{\lambda}_L^{B_2}} \right) \left(\frac{1}{\bar{\lambda}_L^{B_2}} \right) \quad \text{for } 0.43 < \bar{\lambda}_L < 0.6 \quad (6)$$

$$A = (1 - \bar{\lambda}_0^{B_2}) \bar{\lambda}_0^{B_2} \quad (7)$$

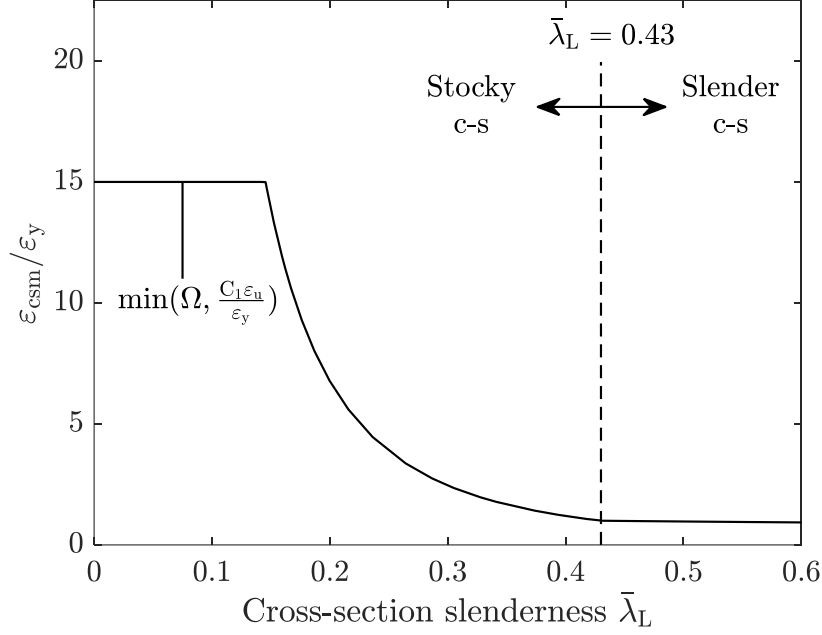


Figure 4. Base curve proposed by Meng et al. (2019).

The cross-section slenderness $\bar{\lambda}_L$ is a parameter that defines the vulnerability to local buckling and it is defined by Equation (8), where f_y is the material yield strength and σ_{cr} is the elastic critical buckling stress of the full cross-section. The latter for the case of CHS is calculated by Equation (9) where E is the Young modulus, ν is the Poisson's ratio, r is the outer radius and t is the wall thickness of the CHS.

$$\bar{\lambda}_L = \sqrt{\frac{f_y}{\sigma_{cr}}} \quad (8)$$

$$\sigma_{cr} = \frac{E}{\sqrt{3(1-\nu^2)}} \left(\frac{t}{r}\right) \quad (9)$$

4.2.2 Material model

A material model capable to capture the post-yielding behaviour is needed. The material model for hot-rolled steel and cold-formed steel have been established by Yun & Gardner (2017) and Yun & Gardner (2018) respectively. The constitutive model proposed for the hot-rolled steel is the quad-linear material model. It is illustrated in Figure 5 (Yun & Gardner, 2017) and it will be used in the present paper. In order to fully describe the stress-strain curve only three parameters are actually needed: the yield stress f_y , the ultimate stress f_u and the Young modulus E . The stress-strain relationship is defined by four stages in Equation (10), where the ultimate strain ϵ_u is expressed in Equation (11), ϵ_{sh} is the value at which the strain hardening starts and it is determined by Equation (12) and E_{sh} is the strain hardening modulus established by Equation (13). Finally, C_1 and C_2 are two material coefficients defined by Equation (14) and (15) respectively.

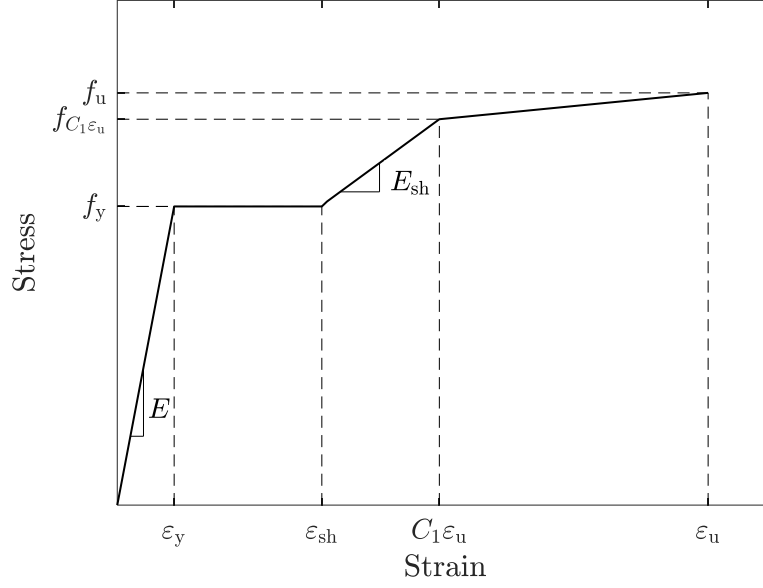


Figure 5. Quad-linear material model for hot-rolled steel.

$$f(\varepsilon) = \begin{cases} E\varepsilon & \text{for } \varepsilon \leq \varepsilon_y \\ f_y & \text{for } \varepsilon_y \leq \varepsilon \leq \varepsilon_{sh} \\ f_y + E_{sh}(\varepsilon - \varepsilon_{sh}) & \text{for } \varepsilon_{sh} \leq \varepsilon \leq C_1\varepsilon_u \\ f_{C_1\varepsilon_u} + \frac{f_u - f_{C_1\varepsilon_u}}{\varepsilon_u - C_1\varepsilon_u}(\varepsilon - C_1\varepsilon_u) & \text{for } C_1\varepsilon_u \leq \varepsilon \leq \varepsilon_u \end{cases} \quad (10)$$

$$\varepsilon_{sh} = 0.1 \frac{f_y}{f_u} - 0.055 \quad \text{but } 0.015 \leq \varepsilon_{sh} \leq 0.03 \quad (11)$$

$$\varepsilon_u = 0.6 \left(1 - \frac{f_y}{f_u}\right) \quad \text{but } \varepsilon_u \geq 0.06 \quad (12)$$

$$E_{sh} = \frac{f_u - f_y}{C_2\varepsilon_u - \varepsilon_{sh}} \quad (13)$$

$$C_1 = \frac{\varepsilon_{sh} + 0.25(\varepsilon_u - \varepsilon_{sh})}{\varepsilon_u} \quad (14)$$

$$C_2 = \frac{\varepsilon_{sh} + 0.4(\varepsilon_u - \varepsilon_{sh})}{\varepsilon_u} \quad (15)$$

In the present paper grade S355 steel is used, where the parameters for the proposed material model are presented in Table 1 (Yun & Gardner, 2017).

Table 1: Key parameters for the quad-linear material model.

Steel grade	E (N/mm ²)	f_y (N/mm ²)	f_u (N/mm ²)	ε_y (%)	ε_{sh} (%)	ε_u (%)	E_{sh} (N/mm ²)	C_1
S355	210,000	355	490	0.17	1.74	16.53	2283	0.38

4.3 Strain averaging approach

In the proposed design approach, the CSM strain limit ε_{csm} is applied to the outer-fibre compressive strain ε_{Ed} in the beam FE model as shown in Equation (16). However, in the Beam FE models the section points within the cross-section are used to extract the individual strain outputs. Therefore the ε_{csm} will be applied to the section point located along the centreline of the cross-section wall thickness.

$$\frac{\varepsilon_{Ed}}{\varepsilon_{csm}} \leq 1 \quad (16)$$

The most severe cases where the yielding is distributed over the full length of the member are the uniform bending and uniform compression. In other cases, such as the three-point bending there is the presence of a strain gradient. The latter is due to the local moment gradient which has a beneficial effect on the local stability of the cross-sections. To account for this benefit, the ‘strain averaging approach’ is applied averaging the strains along a member length equal to the local buckling half-wavelength $L_{b,cs}$. The latter is considered for the analysis referring to some experimental results where the local buckling is defined as the failure criteria of the member (Lay & Galambos, 1964). More precisely, the combination of local and lateral buckling leads to out-of-plane deformations, but the local buckling will start triggering earlier because the lateral buckling requires a wider yielded length along the member (Lay & Galambos, 1964). According to Lay and Galambos (1964) the yielded region of the beam where local buckling will start to occur in the case of moment gradient is identified by two ends, one adjacent to the elastic region and the other one close to the point where the load is applied. Eventually, the location of the strain averaging length corresponds to the part of the beam where there is the highest bending moment. For the case of three-point bending this region will start from mid-span and have an extension equal to the local buckling half-wavelength from both sides of the point load applied at the centre of the beam. Therefore, the strain averaging approach extends the concept of only considering the peak compressive strain expressed in Equation (16). Accordingly, the strain contributions ε_i of n elements located within the local buckling half-wavelength will be considered as shown by Equation (17) and (18) where $\varepsilon_{Ed,Lb}$ is the averaged design strain (Fieber, Gardner & Macorini, 2019a).

$$\frac{\varepsilon_{Ed,Lb}}{\varepsilon_{csm}} \leq 1 \quad (17)$$

$$\text{Where } \varepsilon_{Ed,Lb} = \frac{1}{n} \sum_{1}^n \varepsilon_i \quad \text{and } n \geq 1 \quad (18)$$

Contrarily, the beneficial effect of the local moment gradient would be ignored applying the CSM strain limit only to the peak compressive strain. In addition, the strain averaging approach

defines the maximum element length for the mesh of the model which has to be equal to the local buckling half-wavelength $L_{b,cs}$. An integer number of elements within $L_{b,cs}$ will be considered to extract and average the strains. Formulae to define the local buckling half-wavelength under different loading conditions exists in literature for I-sections and box-sections (Fieber, Gardner & Macorini, 2019b). For CHS a local buckling half-wavelength $L_{b,cs} = 2.444\sqrt{rt}$ for the case of bending is considered in the present paper (Rotter, Sadowski & Chen, 2014). In Figure 6 the effect of the local moment gradients on the ultimate moment capacity is assessed for a CHS class 1 with a local slenderness $D/t\varepsilon^2$ equal to 18.9. The ratio L/D where L is the full length and D the outer diameter (which is here considered equal to 100 mm) varies from 5 to 20. As shown in Figure 6, the shell FE model is able to capture the beneficial effect of the local moment gradients as the member length shortens. In fact, the shell FE model captures an increase in the bending moment capacity of 18% as the length decreases from $L/D = 20$ to $L/D = 5$. Using the beam FE model and averaging the strains along the local buckling half-wavelength $L_{b,cs}$ of the member the same is simulated. However, reducing the length, the increase of ultimate moment capacity is lower compared to the shell FE results. In general, shorter members will have steeper moment gradient and therefore they will perform better in terms of ultimate moment capacity. Indeed, moving away from middle-span the material is at lower stress level and it helps to support the yielded region in the middle of the beam. However, for very long span the local moment gradient converges to zero and, accordingly, the member acts more similarly as it was subjected to uniform bending. A good accordance is obtained between the shell FE results and the Beam FE results with CSM strain limits as shown in Figure 6, but the shell FE results have a significantly higher ultimate moment capacity. The latter, considering only the critical element at mid-span in the beam FE model (not using the strain averaging approach), is investigated in the same figure: it can be noticed that there is no change on the ultimate moment capacity varying the length of the beam. Therefore, the use of the strain averaging approach is more accurate and consistent with the shell FE results and permits to capture the beneficial effects of the moment gradients. Conversely, the EN 1993-1-1 (2005) completely disregards this effect and predicts a constant ultimate moment capacity for all member lengths.

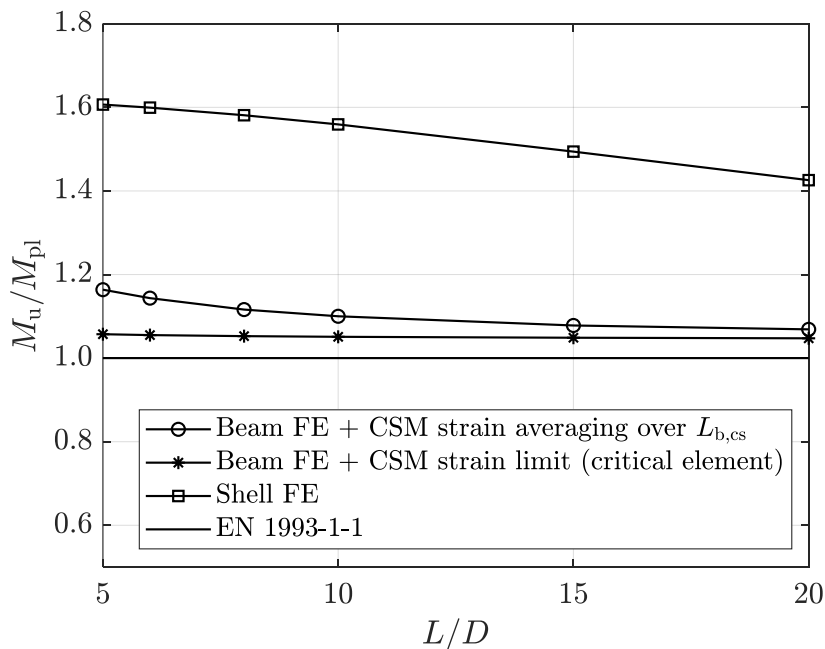


Figure 6. Normalised bending moment capacity for a CHS beam considering different levels of moment gradient.

4.4 Shear resistance check

The presence of the moment gradient implies the interaction of the shear which does not have a beneficial effect and for this reason further checks need to be made. The EN 1993-1-1 (2005) requires undertaking a shear capacity check which prescribes the design shear force V_{Ed} to be minor or equal to the plastic shear capacity $V_{pl,Rd}$. The latest is given by the Equation (19), where A_v is the shear area and γ_{M0} is the partial factor for resistance of cross-sections.

$$V_{pl,Rd} = (A_v f_y / \sqrt{3}) / \gamma_{M0} \quad (19)$$

When cross-sections are subjected to both bending and shear at the same time, considering the EN 1993-1-1 (2005), some checks need to be assessed. There can be two situations, either the design shear force V_{Ed} is less than 0.5 the plastic shear capacity $V_{pl,Rd}$ and the entire moment resistance can be reached or V_{Ed} is bigger than $0.5V_{pl,Rd}$ and the full moment resistance cannot be achieved. In the second case, a reduced moment resistance will be worked out, considering the reduction factor expressed by the Equation (20), also featured in the EN 1993-1-1 (2005) and a reduced yield strength $(1 - \rho)f_y$.

$$\rho = \left(\frac{2V_{Ed}}{V_{pl,Rd}} - 1 \right)^2 \quad (20)$$

Considering the proposed approach of second order inelastic analysis the interaction of shear and bending is taken into account through the reduction factor ρ_{csm} given by Equation (21) that will be applied to the CSM strain limit ε_{csm} .

$$\rho_{csm} = \begin{cases} 1 & \text{for } V_{Ed} \leq 0.5V_{pl,Rd} \\ \frac{0.5}{0.5 + \rho} & \text{for } V_{Ed} \geq 0.5V_{pl,Rd} \end{cases} \quad (21)$$

The check that the cross-section must satisfy is therefore expressed in the Equation (22).

$$\frac{\varepsilon_{Ed}}{\rho_{csm} \varepsilon_{csm}} \leq 1.0 \quad \text{for } V_{Ed} > 0.5V_{pl,Rd} \quad (22)$$

The shear check required by the Eurocode (i.e. $V_{Ed}/V_{pl,Rd} \leq 1$) is still necessary within the proposed analysis. It is also important to mention that for CHS slendernesses $(D - t)/t\varepsilon^2 \geq 100$ the shear buckling must be assessed according to EN 1993-1-6 (2007). In Figure 7 a CHS class 1 with local slenderness $D/t\varepsilon^2$ equal to 18.9 varying the member length is illustrated. Observing the shell FE results, the ultimate moment capacity starts to sharply drop at $L/D = 3$ because of the presence of the shear that starts triggering. Conversely, the beam FE model itself predicts very unconservative ultimate moment capacity compared to the shell FE results. To obtain safe sided predictions that are comparable to shell FE results the shear reduction factor ρ_{csm} needs to be applied to the CSM strain limit in the region of the moment-shear interaction and a shear check is also performed. Thereby, this approach allows to obtain significantly higher ultimate moment capacity than the EN 1993-1-1 (2005) predictions as shown in Figure 7.

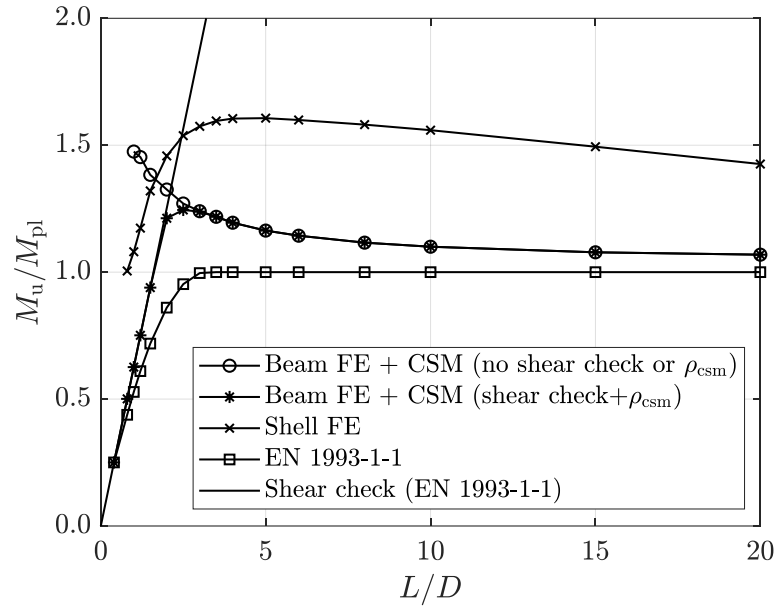


Figure 7. Effect of the shear on the ultimate moment capacity of a CHS with $D/t\epsilon^2 = 18.9$ varying the member length.

A range of CHS beams subjected to three-point bending (with local slenderness $D/t\epsilon^2 \leq 100$ to avoid shear buckling) and varying the member length is investigated. The normalised moment-shear interaction diagram is illustrated in Figure 8 where V_u is the ultimate FE shear capacity. The length range goes from $L/D = 1$ to $L/D = 15$, where D is equal to 100 mm and the cross-sections slendernesses $D/t\epsilon^2$ investigated are equal to 18.9, 30.3, 37.9, 50.5, 75.8, 101.0. In Figure 8 the prEN 1993-1-1 (2020) moment-shear interaction curve appears to be very conservative compared to beam FE results. The reason is because the favourable effect of local moment gradient and the strain hardening are not considered in the Eurocode. As illustrated in Figure 8, in reality the benchmark shell FE results for very short member lengths go beyond the plastic shear resistance. However, the proposed method does not allow it because the plastic shear resistance is the absolute limit that cannot be exceeded.

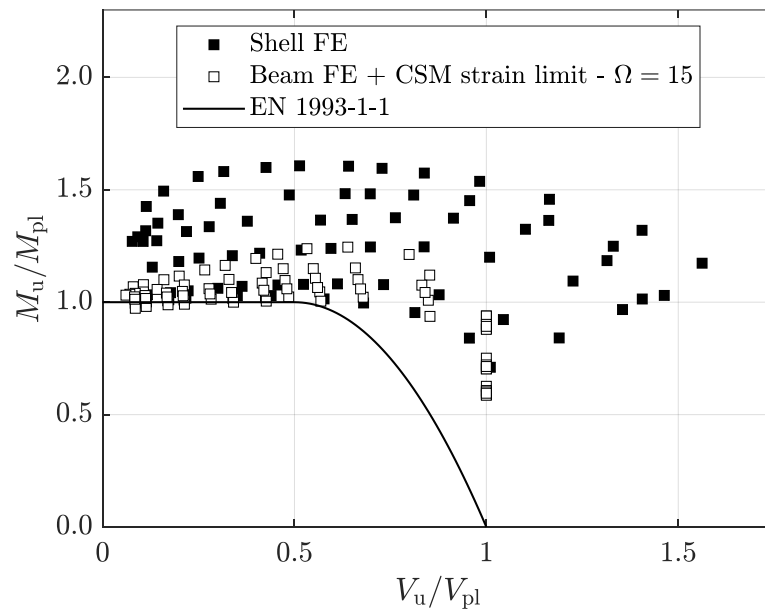


Figure 8. Moment-shear interaction curve for CHS beams predicted by Shell FE model, Beam FE model with CSM strain limit and EN 1993-1-1.

4.5 Initial geometric imperfections and residual stresses

Members imperfections need to be considered because they affect the ultimate capacity of columns. The initial out-of-straightness and residual stresses can be easily modelled through the member geometry. In the EN 1993-1-1 (2005) some equivalent bow imperfections are featured to implicitly consider these imperfections, but they are limited for use with second order elastic analyses. Therefore, they cannot be used in second order inelastic analyses because they would lead to inaccurate predictions of buckling resistance. Moreover, the beam FE model cannot establish local imperfections which is the reason of no local failure. In order to overcome this shortcoming some equivalent bow imperfections have been defined by Walport et al. (2020) for use with second order inelastic analyses. The normalised equivalent bow imperfection magnitude e_0/L is defined in Equation (23), where L is the member length and α is the imperfection factor (Walport, Gardner & Nethercot, 2020). It is important to remark that the consequence of residual stresses and initial imperfections are already considered within the CSM strain limits.

$$\frac{e_0}{L} = \frac{\alpha}{150} \quad (23)$$

5. Application of the proposed design method

In this section the advanced inelastic analysis with CSM strain limits is applied considering CHS members subjected to uniform bending and to three-point bending and the accuracy of the method is assessed. The beam FE models are performed with the software for finite elements Abaqus (ABAQUS, 2014). The results obtained are compared to the benchmark shell FE models described in section 3 and to the current Eurocode provisions in EN 1993-1-1 (2005). The geometric input data for a CHS that have to be defined in accordance with the Abaqus Manual are the outer radius r and the thickness t (ABAQUS, 2014). Other section properties required are the area, the second moment of inertia and the plastic modulus of the CHS to define the applied load. From the beam element library, a 2-node linear pipe is considered (PIPE31). The distinction between the thick-walled pipe assumptions and thin-walled pipe assumptions needs to be made depending on the cross-section thickness. The mesh discretisation of the beam FE models is performed such as the element length is the same as in the shell FE models described in section 3. Moreover, engineering stresses and strains have been incorporated in the Beam FE models as in the Shell FE models. The number of section points for the integration within the CHS have been increased with respect to the standard number to get the gradual spread of plasticity through the cross-sections. In accordance with the Abaqus Manual, for the case of the thick-walled pipe assumptions, at least 3 points in the radial direction and 8 points in the circumferential direction are required. For thin-walled assumptions there are only 8 points in the circumferential direction (ABAQUS, 2014). Some trials increasing the section points in the circumferential direction have been made to obtain a smoother decrease in stiffness from the linear to the non-linear part of the beam model path. Figure 9 illustrates how the increase of section points allows to have a smoother strain hardening through the cross-section, reaching more closely the M_{pl} . Therefore, as shown in Figure 9, 40 section points in the circumferential direction permit to obtain a more accurate result.

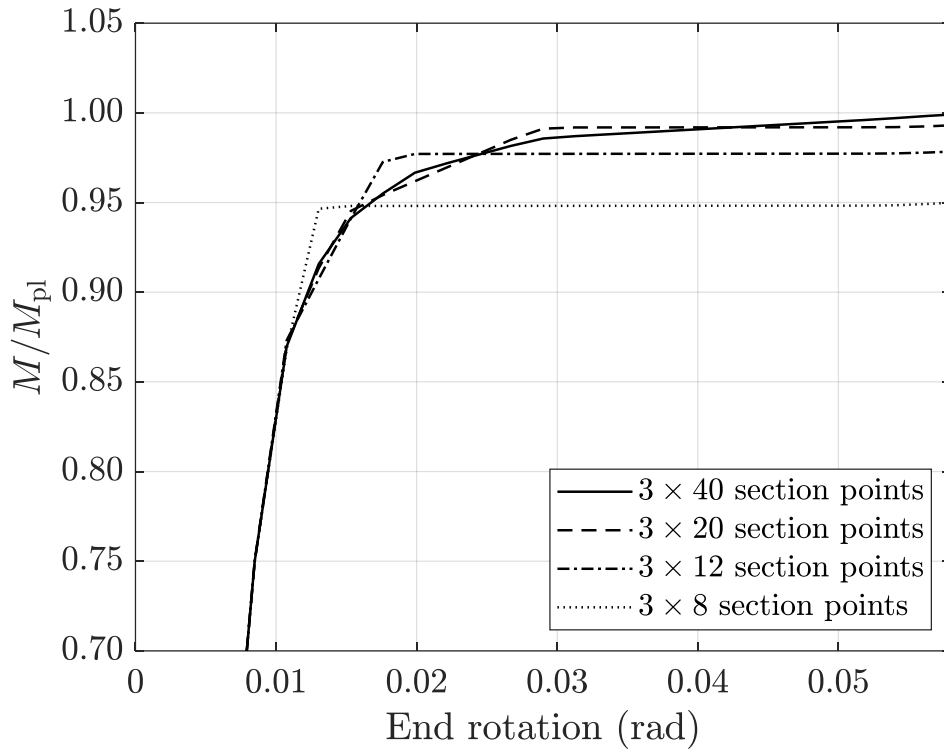


Figure 9. Beam model paths increasing the section points in the circumferential direction.

The value attained in each plateau in Figure 9 is also assessed calculating each area in which the CHS was divided: the case of 3×8 section points is shown in Figure 10 where the entire cross-section is divided in 8 areas and three section points are represented along the CHS wall thickness within each area.

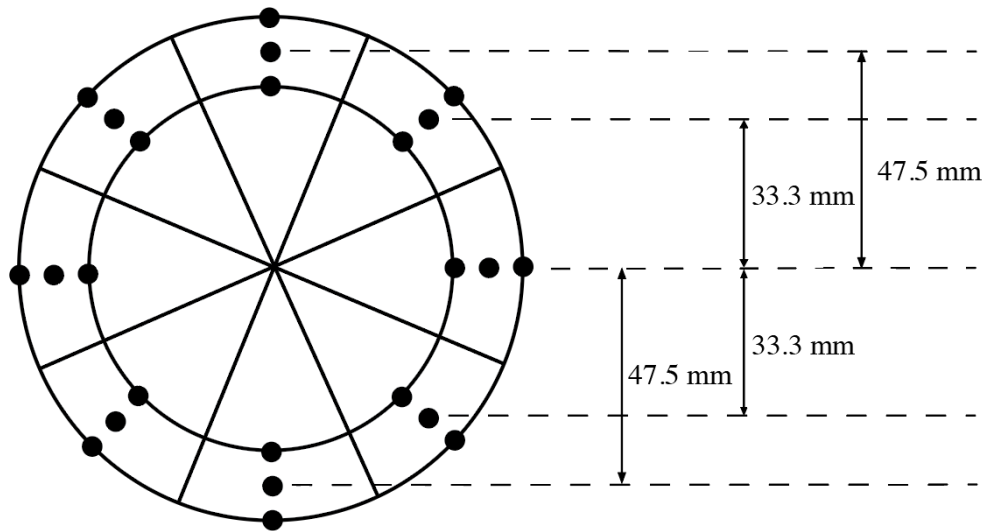


Figure 10. CHS considering thick-walled assumptions with 3×8 section points.

The moment attained in the plateau in Figure 9 is worked out by hand calculating: (1) each area, (2) the corresponding stress extracted at the section point in the middle of the cross-section wall thickness in Figure 10 and (3) the level arm from the centre of the CHS to the centre of each area. Considering the 3×8 path, the value calculated differs from the one reached in Figure 9 only by 0.53%. This result confirms the accuracy that it is obtained from the Beam FE path using the software Abaqus (2014). Furthermore, increasing the number of section points, the

accuracy of the moment calculation improves and get closer to the value of the plateau, therefore, closer to M_{p1} . For both thin-walled pipe and thick-walled pipe assumptions a number of section points equal to 40 has been used in the circumferential direction (ABAQUS, 2014). Moreover, the quad-linear material model for hot-rolled steel described in section 4.2.2 and a steel grade S355 are used to the beam FE model.

5.1 Member subjected to uniform bending

In this section the ultimate bending moment capacity for a range of CHS beams subjected to uniform bending is investigated using the second order inelastic analysis with CSM strain limits. The CHS local slendernesses considered in the investigation vary between $12 \leq D/t\varepsilon^2 \leq 233$. The analysis is restrained to local slenderness $D/t\varepsilon^2 < 240$ which is the limit of applicability for CHS according to prEN 1993-1-1 (2018). In the present study the outer diameter D of the CHS is set to 100 mm and the thickness t varies to achieve a broad range of slendernesses $D/t\varepsilon^2$. The member length is also investigated to find the value which most accurately represents the ultimate moment capacity for different cross-section slendernesses. Firstly, the member length L was set to a value of $5D$ which is long enough to allow local buckling to trigger the member. Eventually, the length has been increased to a value of $10D$ because it is more appropriate to account for the ovalisation effects (Rotter, Sadowski & Chen, 2014). Accordingly, the length $L = 10D$ has been compared with the longest cylinder domain which corresponds to a dimensionless length Ω , as defined in Equation (24), equal to 7 (Rotter, Sadowski & Chen, 2014). The comparison has been conducted to consider the effect of the ovalisation, as it is known that for Ω equal to 7 its influence is most severe. Results showed that the ultimate moment capacity for a length equal to $10D$ and for a dimensionless length Ω equal to 7 differ only by 0.04% and, for this reason, a member length equal to $10D$ is appropriate to perform the analysis.

$$\Omega = \frac{L}{D} \sqrt{\frac{8t}{D}} \quad (24)$$

Application of the second order inelastic analysis with CSM strain limits is illustrated in Figure 11 for the case of a simply supported beam subjected to uniform bending, considering thick-walled assumptions for the beam FE model. The cross-section modelled is Class 1 with a local slenderness $D/t\varepsilon^2 = 18.9$. Therefore, the EN1993-1-1 (2005) cross-section classification predicts a bending moment resistance equal to M_{p1} . Moreover, it has been assessed that the initial stiffness EI/L perfectly matches the linear part of the both the beam and the shell FE models and their paths start to diverge from the M_{el} as shown in Figure 11. The beam FE model keeps deforming with increasing load without reaching any peak because it cannot capture local buckling. Instead, the shell FE model will attain a peak and then the moment capacity will starts decreasing. Since the beam FE model cannot capture local buckling, the CSM strain limit is applied to the outer compressive fibre of the cross-section of the beam FE model, in order to capture the cross-section failure. Comparing the ultimate moment capacity from the beam FE model and the shell FE model, Figure 11 shows that the CSM approach allows to reach a good agreement between the two models. The ultimate moment capacity reached by the beam FE model with the CSM strain limits is slightly higher than the Eurocode prediction. This is thanks to the strain hardening. In reality, shell FE models can predict higher ultimate moment capacity compared to the EN1993-1-1 (2005). Consequently, the Eurocode provisions are considered more conservative because they disregard the strain hardening and the spreading of plasticity.

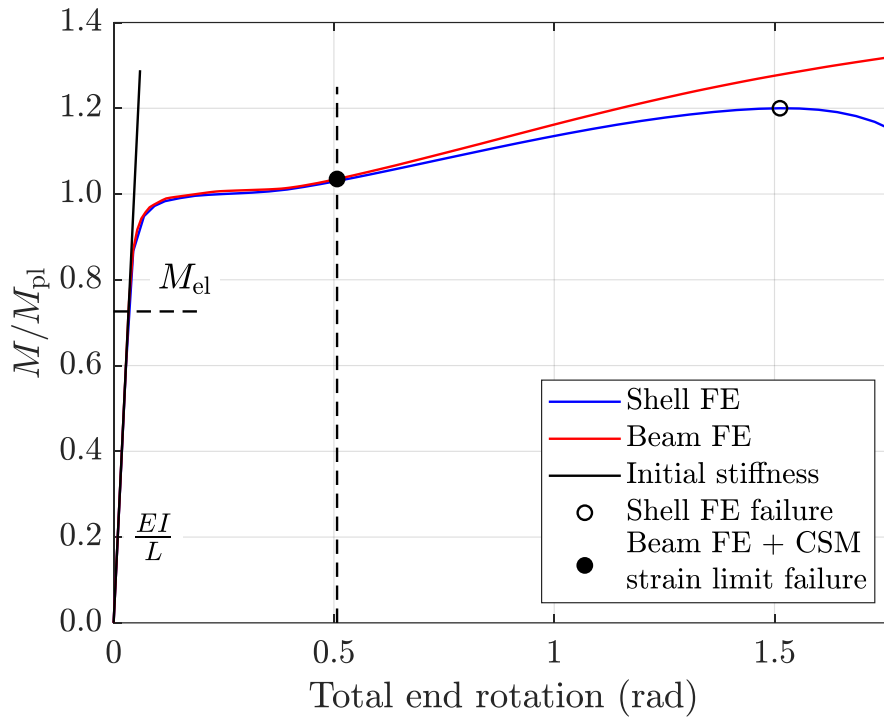


Figure 11. Result of a CHS beam subjected to uniform bending considering thick-walled assumptions.

Another example, considering thin-walled assumptions, is displayed in Figure 12. The cross-section modelled is Class 4 and, therefore, the EN1993-1-1 (2005) cross-section classification predicts a bending moment resistance equal to M_{eff} . Also in this case the initial stiffness EI/L perfectly matches the linear part of both models and their paths start to diverge from the M_{el} .

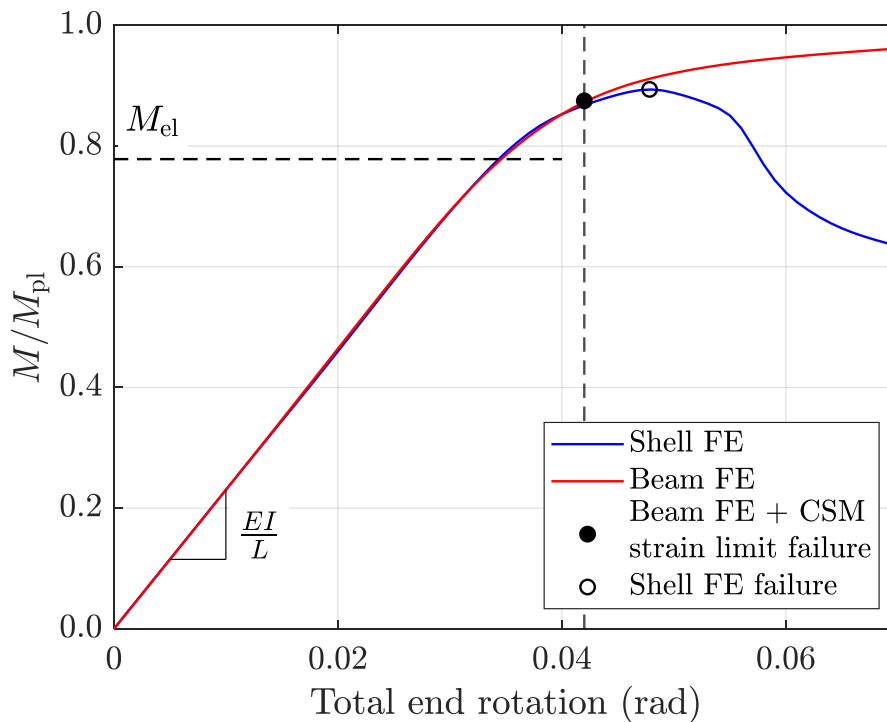


Figure 12. Result of a CHS beam subjected to uniform bending considering thin-walled assumptions.

Eventually the normalised ultimate bending moment capacities M_u/M_{el} where M_{el} is the elastic moment resistance is obtained over a wide range of cross-section slendernesses, as shown in Figure 13. A member length equal to $10D$ is considered and the base curve proposed by Meng et al. (2019) is used to apply the CSM strain limits. Figure 13 also illustrates that the upper limit for the base curve $\Omega = 15$ provides a very conservative ultimate moment capacity for stockier cross-sections. Accordingly, a higher upper limit equal to 30 is investigated to obtain results closer to the benchmark shell FE models. In this way the benefit of the strain hardening is caught for stocky cross-sections with local slenderness $D/t\epsilon^2 < 22$. There is an increase of the ultimate moment capacity of up to 6.7% compared to the Eurocode provisions considering $\Omega = 15$ and an increase of up to 20% considering $\Omega = 30$. Therefore, restricting the upper strain limit to 15 leads to conservative bending moment capacities for stocky cross-sections, however, the results are still above the plastic moment capacity M_{pl} predicted by the Eurocode. The suggested design method, as shown in Figure 13, provides higher ultimate moment capacities in contrast with the EN 1993-1-1 (2005) particularly for more slender cross-sections (class 3 and class 4). Moreover, it is illustrated that the advanced inelastic analysis can precisely predict the same ultimate moment capacity of the benchmark shell FE models for class 2 and 3 cross-sections. However, beam FE results are still very conservative compared to the shell FE for the case of class 4 cross-sections. The latter is due to the inability of the beam FE models to capture local buckling which has an important effect on class 4 cross-sections.

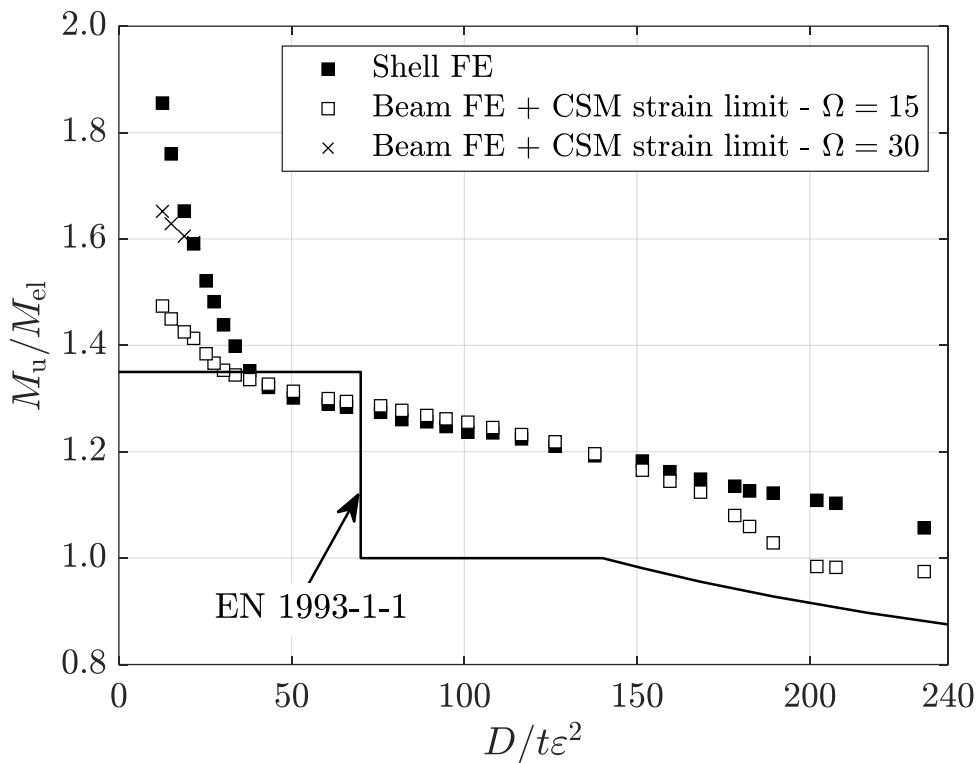


Figure 13. Normalised ultimate moment capacities of CHS beams subjected to uniform bending varying the cross-sections slenderness.

In Table 2 the capacity provisions are summarized and shown for both the suggested design method M_{prop} considering $\Omega = 15$ and the EN 1993-1-1 M_{EC} divided by the shell FE results M_{shell} . It is proved that the Eurocode predictions are more conservative for hot-rolled CHS members. The advanced inelastic analysis with CSM strain limits provides more precise results and it allows to reach higher bending moment capacity than the Eurocode provisions.

Table 2: Capacity predictions using the second order inelastic method M_{prop} and the EN1993-1-1 M_{EC} normalised by the benchmark shell FE results M_{shell} for hot-rolled steel CHS members subjected to uniform bending.

Section type	Load case	Number of CHS	M_{EC}/M_{shell} mean	M_{prop}/M_{shell} mean
CHS	Uniform bending	31	0.86	0.96

A comparison is also conducted between the Beam FE results obtained with the base curve proposed by Meng et al. (2019) and the base curve used by Buchanan et al. (2016). As shown in Figure 14, while the two base curves give similar results for the case of stocky cross-sections, the base curve proposed by Meng et al. (2019) predicts higher ultimate moment capacity for more slender cross-sections and as a result it will be the one used for the analysis.

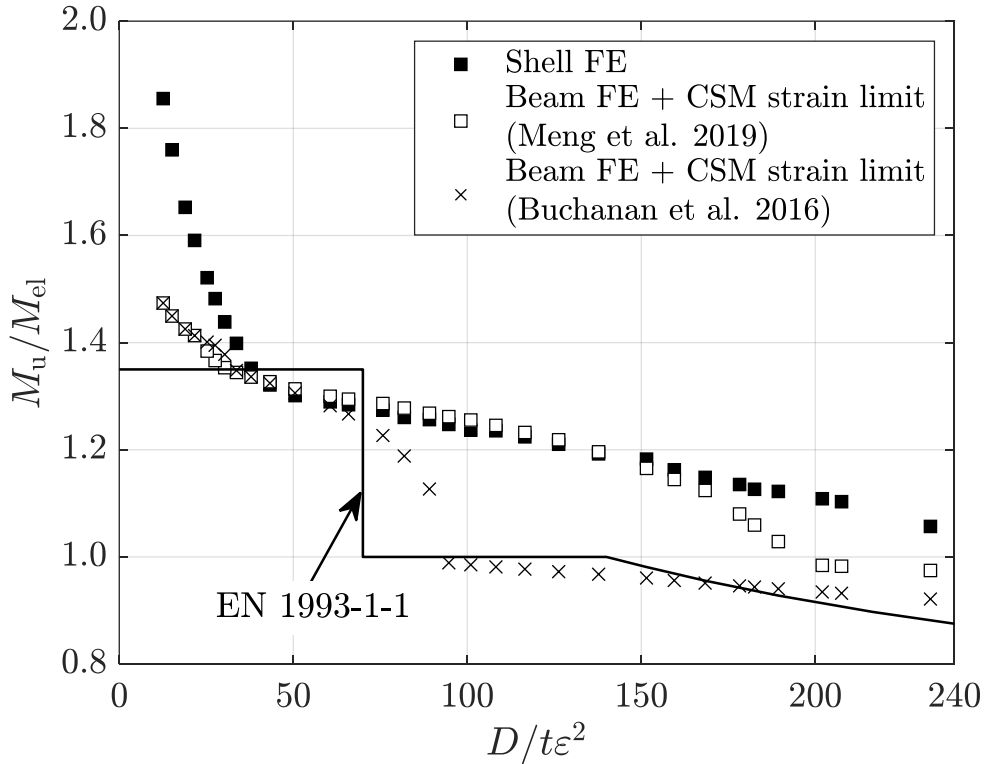


Figure 14. Comparison between Meng et al. (2019) and Buchanan et al. (2016) base curves considering the normalised ultimate moment capacities.

5.2 Member subjected to three-point bending

In this section the application of the second order inelastic analysis with CSM strain limits is conducted on hot-rolled CHS steel members subjected to three-point bending. An example of a simply supported beam under three-point bending is illustrated in Figure 15. The CHS is class 1 and has a local slenderness $D/t\epsilon^2 = 30.3$ with a corresponding CSM strain limit $\epsilon_{csm}/\epsilon_y = 10.59$. The latter is applied to the averaged strains along the local buckling half-wavelength $L_{b,cs}$ of the member as explained in section 4.3 and illustrated in Figure 15. The critical strain averaging length is located from mid-span where the load is applied for an extension equal to $L_{b,cs}$. It is noticeable that, averaging the strain along $L_{b,cs}$, the beam FE ultimate moment capacity is still significantly lower than the shell FE model, but higher than the EN 1993-1-1 (2005). Successively, in the current paper further investigations are conducted varying the critical strain averaging length to assess the more appropriate extension that allows

to obtain a closer agreement between beam FE and shell FE results. Figure 15 displays that the Beam FE model does not attain a peak, but it keeps increasing because it cannot capture local buckling, while the benchmark shell FE model fails at a certain value.

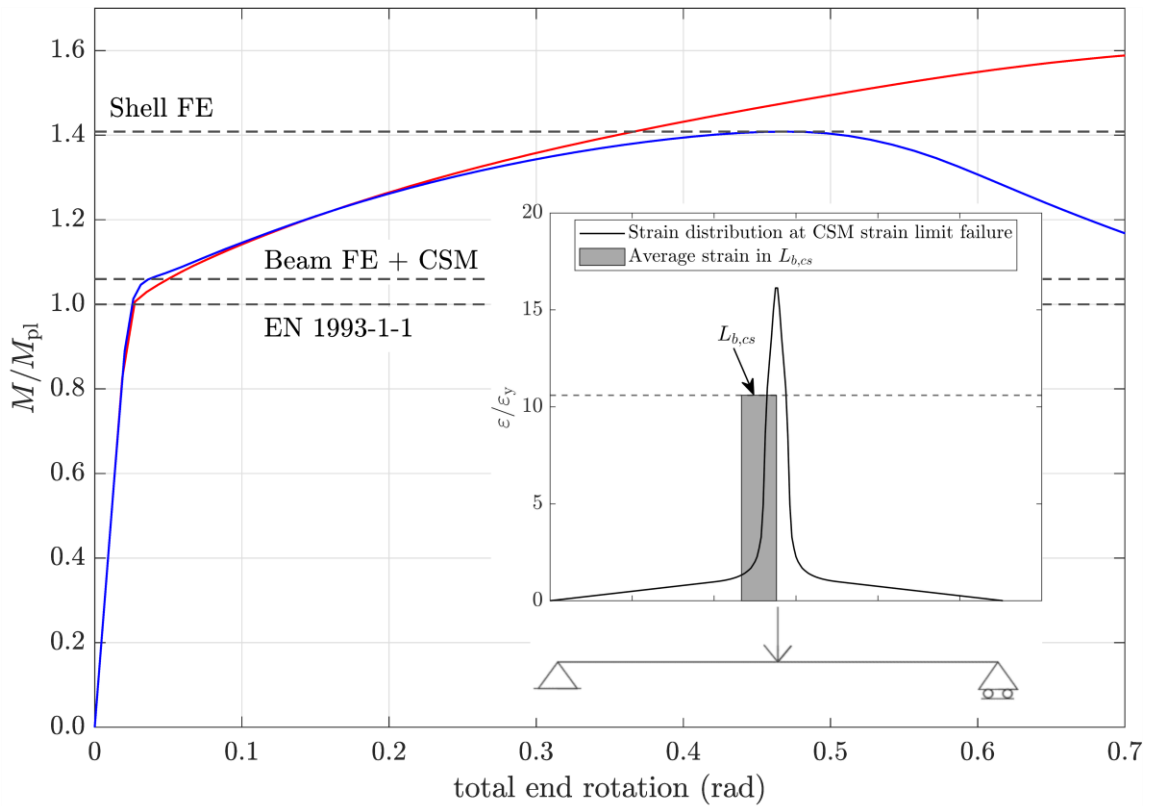


Figure 15. Response of a hot-rolled steel CHS beam with a local slenderness $D/t\varepsilon^2 = 30.3$ subjected to three-point bending.

The ultimate bending moment capacity for a range of cross-section slendernesses $D/t\varepsilon^2$ is initially investigated considering a member length equal to $10L_{b,cs}$, similarly to what was already conducted for I-sections and box-sections (Fieber, Gardner & Macorini, 2019a; Walport, Gardner & Nethercot, 2021). The results demonstrated that for a member length $L = 10L_{b,cs}$ the local moment gradient does not remain constant. In fact, because of the definition of the local buckling half-wavelength $L_{b,cs} = 2.444\sqrt{rt}$, the beam length varies with the cross-section slenderness (Timoshenko & Woinowsky-Krieger, 1959). For thinner tubes the $L_{b,cs}$ is shorter and it leads to a shorter member length, conversely, for thicker tubes the $L_{b,cs}$ is bigger and so also the length of the beam. Therefore, considering the beam extension in function of $L_{b,cs}$ leads to have different moment gradients over a range of cross-sections and consequently it cannot be adopted. Eventually, to keep the moment gradient constant over a series of cross-sections, the member length adopted in the current paper is proportional to the outer diameter D of the CHS. To confirm the above, Figure 16 illustrates how the moment gradient, expressed as the normalised shear over the normalised moment, varies considering the length proportional to the outer diameter D and equal to $10L_{b,cs}$.

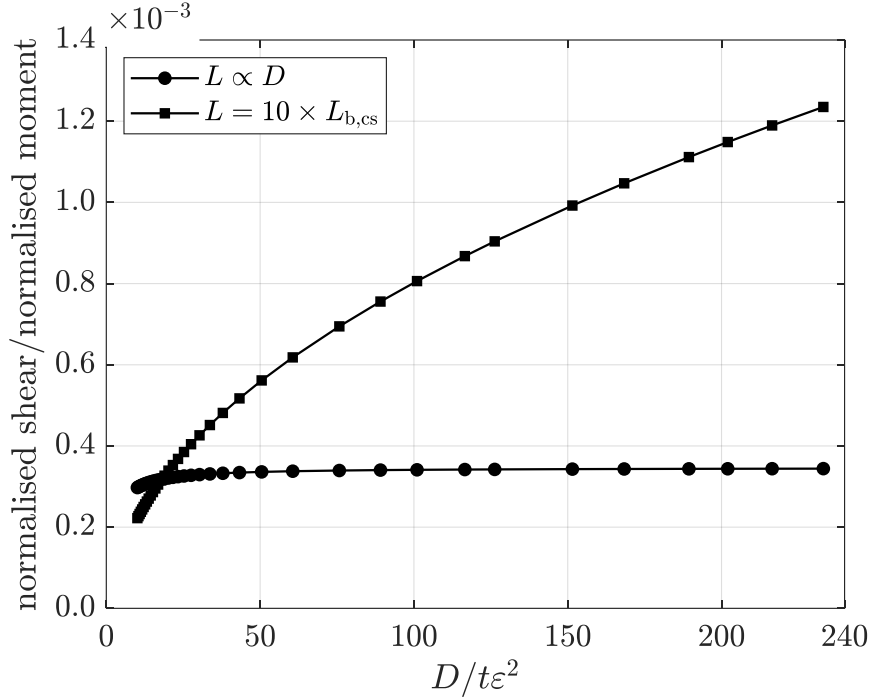


Figure 16. Variation of the moment gradient over a range of cross-section slendernesses.

Therefore, the normalised bending moment capacities M_u/M_{el} , where M_u is the ultimate moment capacity and M_{el} is the elastic moment, for a series of cross-section slendernesses subjected to three-point bending is investigated. To preserve the local moment gradient constant a member length equal to $10D$ (where D is set to a value of 100 mm) is chosen, as shown in Figure 17. As for the uniform bending, also here the upper limit of the base curve for stocky cross-sections $\Omega = 15$ seems to be very conservative and significantly restricts the moment resistance of cross-sections with local slenderness $D/t\epsilon^2 < 22$. To obtain results closer to the shell FE predictions a higher strain hardening is permitted extending the upper limit of the base curve for stocky cross-sections to $\Omega = 30$. While there is an increase of the ultimate moment capacity of up to 14% compared to the Eurocode provisions considering $\Omega = 15$, an increase of up to 29% is obtained considering $\Omega = 30$. In this way a more accurate representation of the benchmark shell FE results is attained for stockier cross-sections. Moreover, as the cross-section slenderness increases there is a gradual decrease of the ultimate moment capacity which is precisely contemplated by the CSM strain limits. Additionally, it can be seen in Figure 17 that the proposed method with CSM strain limits predicts a higher ultimate moment capacity compared to the EN 1993-1-1 (2005) provisions. The sharp jump in the EN 1993-1-1 (2005) from M_{pl} to M_{el} that is present between class 2 and class 3 cross-sections is extremely inaccurate compared to the benchmark shell FE results. Indeed, the ultimate moment capacity obtained from the shell FE model slowly and linearly decreases from class 2 to class 3 cross-sections. For this reason, a linear transition proposed by Meng et al. (2020) along the class 3 cross-sections will contribute to a more accurate approximation to the shell FE results. Furthermore, there is a close agreement between the beam FE results with CSM strain limits and the shell FE results only for class 3 cross-sections. For this reason, further investigations are conducted assessing the critical strain averaging length along which to average the strains and to apply the corresponding CSM strain limit. Some comparisons are displayed in Figure 18 where the normalised bending capacities M_u/M_{el} is obtained averaging the strains along one time the local buckling half-wavelength $L_{b,cs}$, two times the $L_{b,cs}$ and four times the $L_{b,cs}$ of the member. The corresponding strain distributions for the three different strain averaging lengths are shown

in Figure 19 for a class 1 cross-section with local slenderness $D/t\varepsilon^2 = 30.3$ and a corresponding CSM strain limit $\varepsilon_{\text{CSM}}/\varepsilon_y = 10.59$ to exemplify the approach used in the proposed method. The ultimate moment capacity is also plotted considering only the strain of the critical element at mid-span without applying the strain averaging approach. Potentially, increasing the length along which to apply the strain averaging approach the normalised bending capacities M_u/M_{el} should grow because of the presence of a strain gradient along the member length. The beam subjected to the three-point bending presents a yielded region close to mid-span, but the strains further from the applied load do not reach the yield point and therefore they enable the member to attain a higher ultimate moment capacity. As illustrated in Figure 18, there is a slightly gain of ultimate moment capacity if the strain averaging approach is used in place of applying the CSM strain limit at the critical element at mid-span. Generally, as the critical strain averaging length increases the ultimate moment capacity grows. From the results obtained the latter is more significant for stockier cross-sections. For class 3 and class 4 cross-sections, averaging the strains along a longer length, does not provide an important increasing on their ultimate moment capacities.

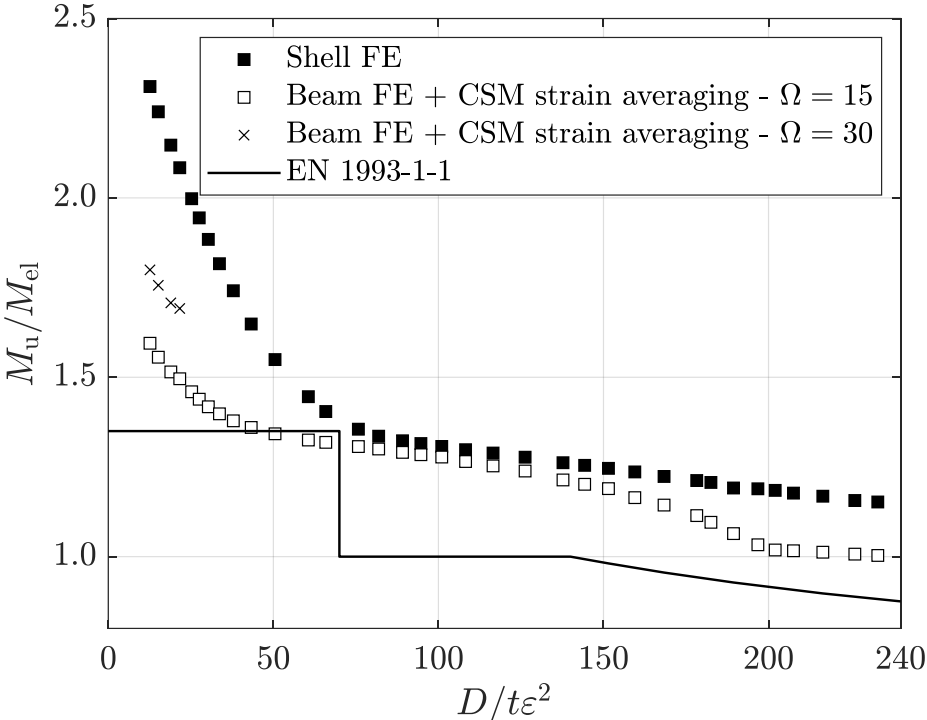


Figure 17. Normalised ultimate moment capacities of CHS beams subjected to three-point bending varying the cross-section slenderness.

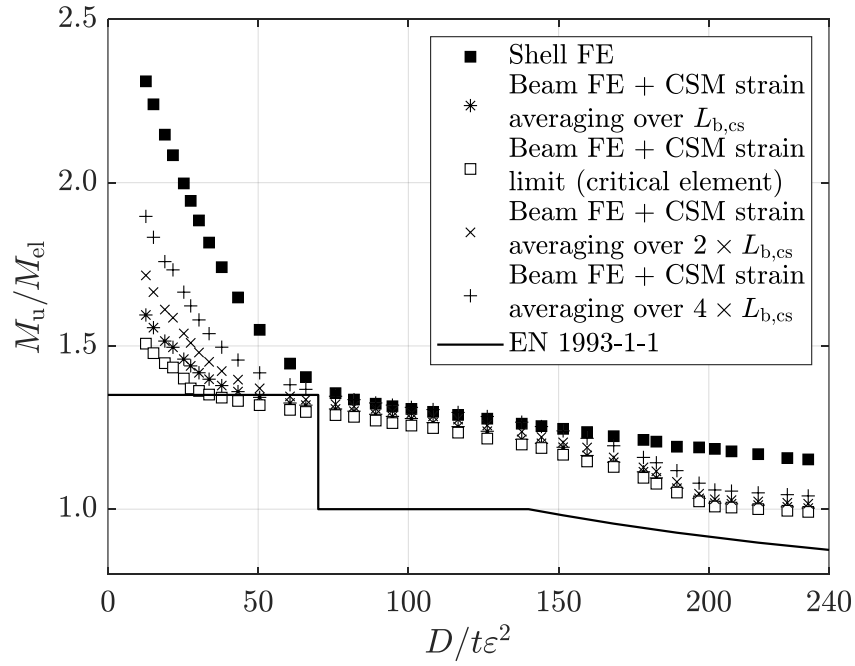


Figure 18. Normalised ultimate moment capacities of CHS beams subjected to three-point bending varying the cross-section slenderness and the strain averaging length.

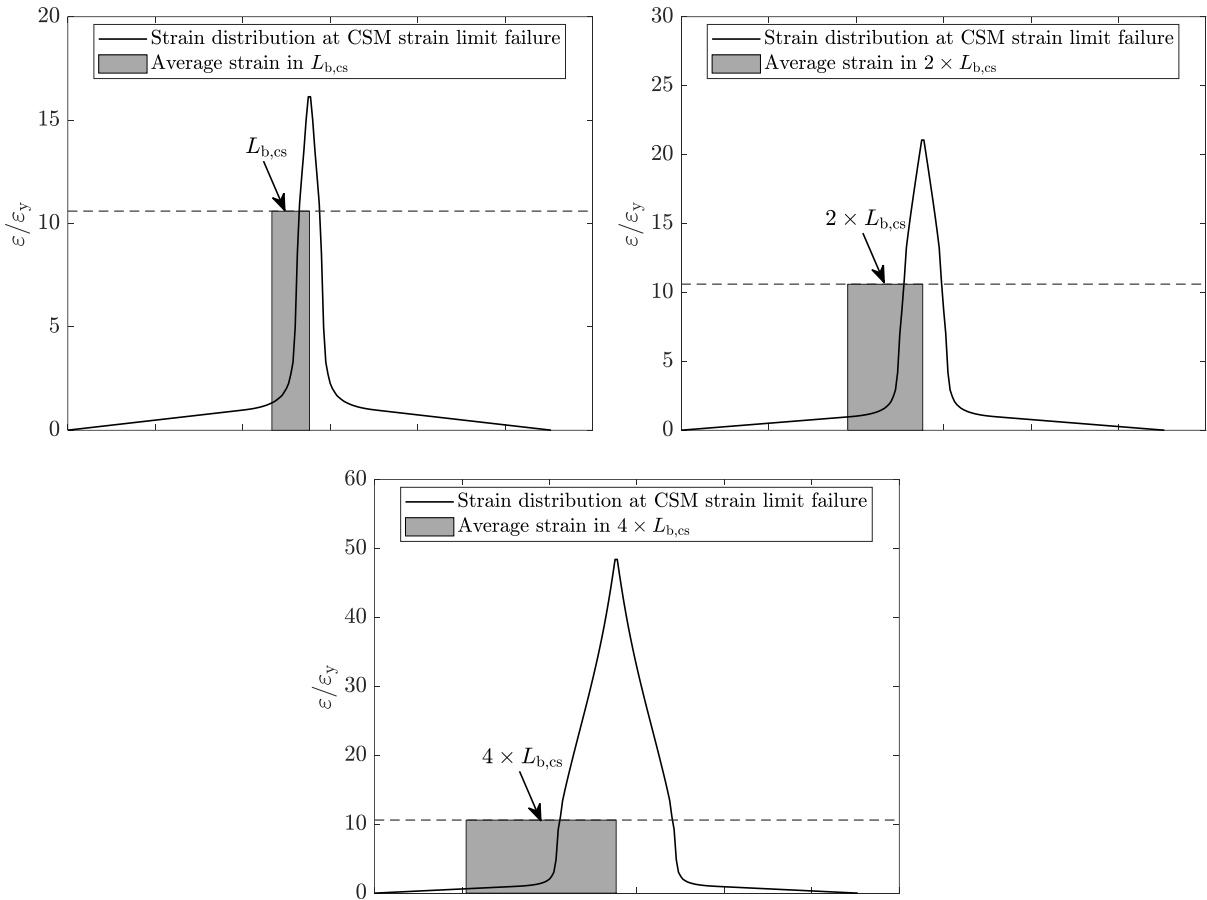


Figure 19. Strain distributions for a Class 1 CHS with local slenderness $D/t\epsilon^2 = 30.3$ and CSM strain limit $\epsilon_{csm}/\epsilon_y = 10.59$ considering the strain averaging length equal to $L_{b,cs}$ (on the top left), $2 \times L_{b,cs}$ (on the top right) and $4 \times L_{b,cs}$ (at the bottom centre).

An outline of the capacity provisions is shown in Table 3 for both the suggested design method M_{prop} considering $\Omega = 15$ and the EN 1993-1-1 M_{EC} divided by the shell FE results M_{shell} . The proposed design method M_{prop} is obtained considering the strains averaged along a length equal to $L_{b,cs}$. The proposed method using Beam FE with CSM strain limits allows to reach higher moment capacities respect to the Eurocode predictions. Furthermore, the capacity provisions of the proposed method M_{prop} normalised by the Shell FE results M_{shell} are displayed in Table 4 considering different lengths along which to apply the strain averaging approach.

Table 3: Outline of capacity provisions using the proposed method M_{prop} and the EN1993-1-1 M_{EC} normalised by the benchmark shell FE results M_{shell} for hot-rolled steel CHS members subjected to three-point bending.

Section type	Load case	Number of CHS	M_{EC}/M_{shell} mean	M_{prop}/M_{shell} mean
CHS	Three-point bending	35	0.76	0.87

Table 4: Ultimate bending moment capacity considering the propose method M_{prop} normalised by the Shell FE results M_{shell} applying the strain averaging approach along different lengths.

Strain averaging length	M_{prop}/M_{shell} mean
Critical element	0.86
$L_{b,cs}$	0.87
$2 \times L_{b,cs}$	0.89
$4 \times L_{b,cs}$	0.93

As it is demonstrated in section 5.1 for the case of uniform bending, the base curve proposed by Meng et al. (2019) enables also the members subjected to three-point bending to reach a higher ultimate moment capacity than the base curve introduced by Buchanan et al. (2016). The capacity predictions for stockier cross-sections remain the same for either the two base curves. Conversely, for more slender cross-sections the gain of ultimate moment capacity is significantly higher using Meng et al. (2019) base curve, as displayed in Figure 20. Therefore, it is demonstrated that the base curve proposed by Meng et al. (2019) allows to get a closer agreement to the results obtained from the benchmark shell FE models, at least for more slender cross-sections.

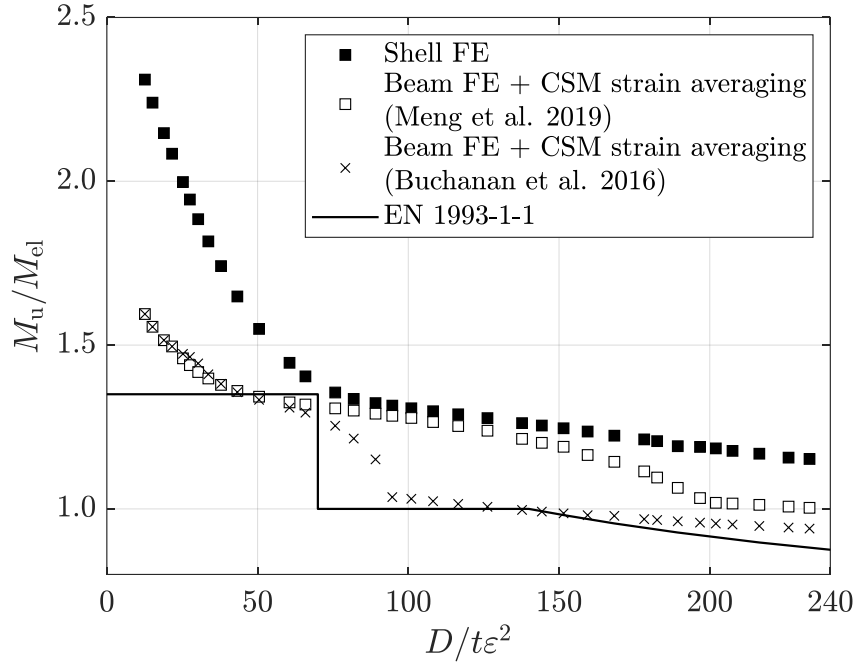


Figure 20. Comparison between Meng et al. (2019) and Buchanan et al. (2016) base curves for the normalised ultimate moment capacities.

5.2.1 Benefits from local moment gradients over uniform bending

Upon collecting the beam FE and shell FE results for both the uniform bending and the three-point bending, some studies proceeded to assess the benefits from the moment gradients over uniform bending. As previously stated, for the case of uniform bending the strain along the member length is uniformly distributed, while for the case of the three-point bending there is a strain gradient along the beam that allows it to reach a higher ultimate moment capacity. As the member length increases, for a beam subjected to three-point bending, the moment gradient closely converges to zero which means that the moment capacity of three-point bending will converge to the uniform bending. To assess the benefits of the local moment gradients the ultimate bending moment capacity M_u^{3pb} for the three-point bending normalised by that under uniform bending M_u^{4pb} is calculated. Figure 21 illustrates the point mentioned above for the case of a stocky and a slender cross-section and it is noticeable that the benefits from the moment gradients over uniform bending is more significant in stocky cross-sections. It is expected that for shorter member lengths there is a drop in the ultimate moment capacity due to the detrimental effect of the shear which starts triggering the beam. For intermediate lengths the negative influence of the shear is compensated by the positive effect of the local moment gradient which allows the modelled beams to reach a significant moment capacity. For longer lengths the three-point bending ultimate capacity starts slowly to converge to the uniform bending because the moment gradient becomes flatter and it will not have beneficial effect anymore. However, in the shell FE models the convergence is significantly slow because of the mid-span stiffener that restrains the ovalisation effect at the centre of the beam and therefore, the ultimate moment capacity will be still high at mid-span. Nonetheless, as the moment gradient becomes flatter increasing the member length, the stiffener should have less effect. Therefore, analysing the buckled shape of long members of the shell FE models, it is assessed that failure does not occur at mid-span (where there is the maximum moment), but at a certain distance away from the critical region where the moment will be smaller. Precisely, for short members, failure arises at mid-span and increasing the length it will occur at a bigger distance away from it, as shown in Figure 22. To take account of the effect of the stiffener and the actual

region where failure occurs, the failure moment M'_u is calculated at the point where the beam actually starts to buckle. The latter is smaller than the one at mid-span and the convergence will be reached more quickly for long members as illustrated in Figure 23. For the case of $L = 200D$ (where D is equal to 100 mm), considering M'_u at the actual point of failure, the three-point bending capacity normalised by the uniform bending result is about equal to 1.03 (3%). Conversely, considering the M_u at mid-span the ratio is higher and equal to 1.08 (8%). This result confirms that to reach more accurately the convergence the ultimate moment capacity has to be considered where failure really arises.

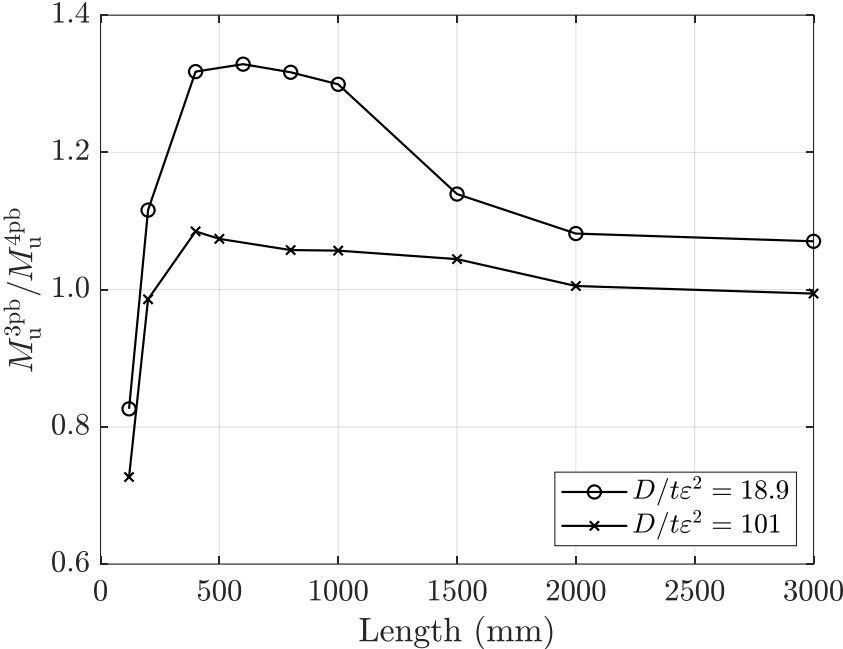


Figure 21. Different benefits from moment gradients for a stocky cross-section and a slender cross-section.

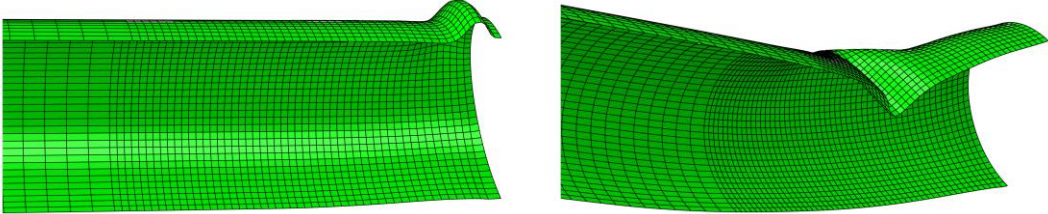


Figure 22. Buckled shapes for a short member (on the left) and for a long member (on the right).

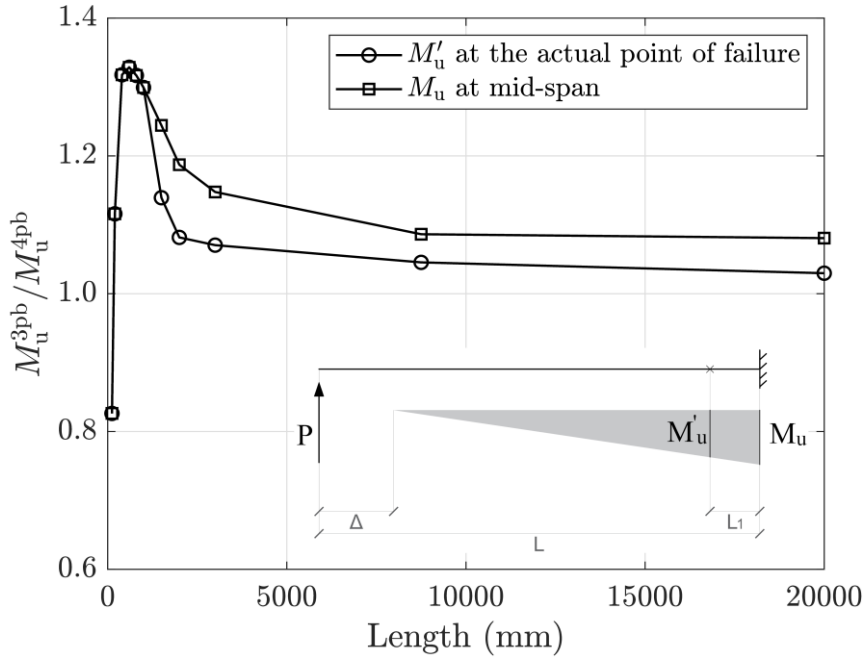


Figure 23. Ultimate bending moment capacity M_u^{3pb} from three-point bending normalised by the uniform bending M_u^{4pb} for a stocky cross-section with $D/t\varepsilon^2 = 18.9$.

An example of what just mentioned previously is illustrated in Figure 24 for the case of a stocky cross-section with $D/t\varepsilon^2 = 18.9$. The moment-ovalisation displacement curve shows how three different member lengths subjected to three-point bending converge to uniform bending. The convergence is reached calculating the ultimate moment capacity at the actual point of the failure as just explained. It is demonstrated that, as the member length increases, convergence to the uniform bending is attained. Moreover, the ovalisation displacement are more significant for longer members.

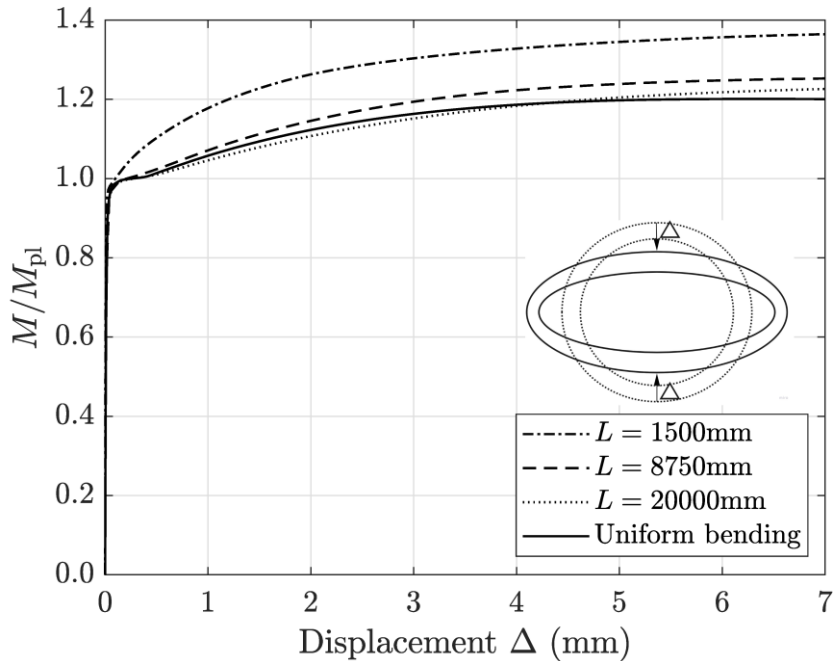


Figure 24. Moment-displacement curve of a stocky cross-section considering the convergence to uniform bending of three member lengths subjected to three-point bending.

6. Conclusions and suggestion for future research

6.1 Conclusion

A second order inelastic analysis for the design of steel frames is presented in this paper focusing on the assessment of hot-rolled CHS steel members subjected to uniform bending and three-point bending. The continuous strength method (CSM) is used to mimic local buckling in the Beam FE models. The CSM strain limits are applied to a characteristic length along the members to consider the benefits achieved from the local moment gradients. Overall, the proposed method using beam finite elements with CSM strain limits predicts more accurate and higher ultimate capacity compared to the EN 1993-1-1 (2005). The latest is significantly noticeable for more slender cross-sections (class 3 and class 4) where the gain of ultimate moment capacity is prominent in contrast to the Eurocode provisions. Moreover, while for the case of uniform bending the ultimate moment capacity from the beam FE model reaches a good agreement with the benchmark Shell FE model, for the three-point bending the results are not as precise. Indeed, the beam FE results for the case of three-point bending proved to be significantly more conservative than the shell FE model for some cross-section slendernesses. Their conservativeness can be generated by the base curve that for some cross-section slendernesses could not reflect the actual deformation capacity. Other major factors which can affect these results are the investigated member lengths that will consequently cause different moment gradients and therefore, different ultimate moment capacities. Moreover, the mesh size and the imperfection shape used have an impact on the outcomes. The conservative ultimate moment capacity from the class 4 cross-sections arises from the fact that beam FE models cannot capture local buckling which has a significant effect on class 4 cross-sections. In addition, the present paper focuses on the impact that the critical strain averaging length has on the ultimate moment capacity. It is demonstrated that averaging the strains along the local buckling half-wavelength $L_{b,cs}$ does not provide an accurate result in terms of ultimate moment capacity compared to the shell FE models. Furthermore, as the critical strain averaging length increases, the capacity prediction grows owing to the presence of the strain gradient. Eventually, only considering the critical strain averaging length equal to $4 \times L_{b,cs}$ permits to reach a closer agreement with the shell FE results. It is also demonstrated that increasing the upper limit of the base curve to $\Omega = 30$ allows stocky cross-sections to reach higher strain hardening and therefore higher ultimate moment capacity. Moreover, the benefit from the moment gradients over uniform bending is evaluated and results show that stockier cross-sections are more affected by the beneficial effect from the moment gradients than slender cross-sections. Additionally, it is assessed in this paper that the base curve for CHS proposed by Meng et al. (2019) predicts a higher ultimate bending moment capacity compared to the base curve by Buchanan et al. (2016). This result is noticeable for more slender cross-sections. In conclusion, the proposed method using beam finite elements permits to have a more computationally efficient analysis as opposed to the use of Shell FE and significant benefit compared to the Eurocode provisions. Therefore, the advanced inelastic analysis with CSM strain limits in contrast with the Eurocode design rules does not require any cross-section classification or individual member checks to assess their stability.

6.2 Suggestion for future research

The current method is presently verified for I-sections and box-sections and it is still underway for CHS steel members. In the present paper only hot-rolled steel and a steel grade S355 is investigated with the use of the quad-linear material model. Further investigations can be conducted regarding different steel grades and cold-formed steel using the bilinear material

model. The stainless steel and the aluminium CHS members can also be assessed using the Ramberg-Osgood material model (Afshan, Zhao & Gardner, 2019). Additional researches can be undertaken for the CHS base curve to obtain a more accurate strain hardening and spreading of plasticity through the stockier cross-section and, in general, a closer agreement with the shell FE results. A further inspection is required to find the most appropriate length to apply the strain averaging approach. Currently the local buckling half-wavelength seems not to capture very significant benefit of the local moment gradient. In fact, the ultimate bending capacity averaging along the local buckling half-wavelength is not sufficiently higher compared to the ultimate capacity obtained by applying the CSM strain limit to the critical element at mid-span. More loading scenarios can also be assessed such as columns subjected to compression and beam-columns with combined compression and bending until reaching structural systems such as frames and continuous beams.

Acknowledgment

The research has been conducted under the supervision of the Professor Leroy Gardner. I am extremely grateful to him for this opportunity. I also want to thank Fiona Walport and Xin Meng for helping me with the beam FE models and Shell FE models respectively. I am also thankful to Politecnico di Torino which gave me the opportunity to spend a year at the Imperial College London and to the Professor Francesco Tondolo who supervised my project from Italy.

References

- ABAQUS. (2014) *Abaqus Analysis User's Guide*. Version 6.14. Providence, RI, USA, Dassault Systemes Simulia Corp. Available from: 130.149.89.49:2080/v6.14/books/usb/default.htm.
- Afshan, S., Zhao, O. & Gardner, L. (2019) Standardised material properties for numerical parametric studies of stainless steel structures and buckling curves for tubular columns. *Journal of Constructional Steel Research*. 152, 2-11. Available from: doi: 10.1016/j.jcsr.2018.02.019.
- British Standards Institute. (1991) BS 4848-2:1991. *Hot-rolled structural steel sections. Specification for hot-finished hollow sections*. London, British Standards Institute.
- British Standards Institute. (1983) BS 6363:1983. *Specification for welded cold formed steel structural hollow sections*. London, British Standards Institute.
- Buchanan, C., Gardner, L. & Liew, A. (2016) The continuous strength method for the design of circular hollow sections. *Journal of Constructional Steel Research*. 118, 207-216. Available from: doi: 10.1016/j.jcsr.2015.11.006.
- Chan, T. M. & Gardner, L. (2008) Bending strength of hot-rolled elliptical hollow sections. *Journal of Constructional Steel Research*. 64 (9), 971-986. Available from: doi: 10.1016/j.jcsr.2007.11.001.
- Chen, M. & Young, B. (2019) Material properties and structural behavior of cold-formed steel elliptical hollow section stub columns. *Thin-Walled Structures*. 134, 111-126. Available from: doi: 10.1016/j.tws.2018.07.055.

European Committee for Standardization. (2005) EN 1993-1-1:2005. *Eurocode 3 - Design of steel structures - Part 1-1: General rules and rules for buildings*. Brussels, European Committee for Standardization.

European Committee for Standardisation. (2007) EN 1993-1-6: 2007. *Eurocode 3 - Design of steel structures - Part 1-6: Strength and Stability of Shell Structures*. Brussels, European Committee for Standardisation.

European Committee for Standardisation. (2018) prEN 1993-1-1:2018. *Eurocode 3 - Design of Steel Structures - Part 1-1: General Rules and Rules for Buildings*. Brussels, European Committee for Standardisation.

European Committee for Standardization. (2020) prEN 1993-1-1:2020. *Eurocode 3 - Design of steel structures - Part 1-1: General rules and rules for buildings*. Brussels, European Committee for Standardization.

Fieber, A., Gardner, L. & Macorini, L. (2020) Structural steel design using second-order inelastic analysis with strain limits. *Journal of Constructional Steel Research*. 168, 105980. Available from: doi: 10.1016/j.jcsr.2020.105980.

Fieber, A., Gardner, L. & Macorini, L. (2019a) Design of structural steel members by advanced inelastic analysis with strain limits. *Engineering Structures*. 199, 109624. Available from: doi: 10.1016/j.engstruct.2019.109624.

Fieber, A., Gardner, L. & Macorini, L. (2019b) Formulae for determining elastic local buckling half-wavelengths of structural steel cross-sections. *Journal of Constructional Steel Research*. 159, 493-506. Available from: doi: 10.1016/j.jcsr.2019.04.037.

Gardner, L. (2008) The continuous strength method. *Proceedings of the Institution of Civil Engineers - Structures and Buildings*. 161 (3), 127-133. Available from: doi: 10.1680/stbu.2008.161.3.127.

Gardner, L., Yun, X., Fieber, A. & Macorini, L. (2019) Steel Design by Advanced Analysis: Material Modeling and Strain Limits. *Engineering*. 5 (2), 253-259. Available from: doi: 10.1016/j.eng.2018.11.026.

Law, K. H. & Gardner, L. (2012) Lateral instability of elliptical hollow section beams. *Engineering Structures*. 37, 152-166. Available from: doi: 10.1016/j.engstruct.2011.12.008.

Lay, M.,G. & Galambos, T.,V. (1966) *The Inelastic behavior of beams under moment gradient*. Lehigh University, Fritzt Engineering Laboratory Report No 297.12.

Meng, X. & Gardner, L. (2020) Simulation and design of semi-compact elliptical hollow sections. *Engineering Structures*. 202, 109807. Available from: doi: 10.1016/j.engstruct.2019.109807.

Meng, X., Gardner, L., Sadowski, A. J. & Rotter, M. J. (2020) Elasto-plastic behaviour and design of semi-compact circular hollow sections. *Thin-Walled Structures*. 148, 106486. Available from: doi: 10.1016/j.tws.2019.106486.

- Meng, X., Toffolon, A., Gardner, L. & Taras, A. (2019) The generalised slenderness-based resistance method for the design of CHS and EHS. *Steel Construction: Design and Research*. 12 (4), 342-353. Available from: doi: 10.1002/stco.201900038.
- Rotter, J. M., Sadowski, A. J. & Chen, L. (2014) Nonlinear stability of thin elastic cylinders of different length under global bending. *International Journal of Solids and Structures*. 51 (15-16), 2826-2839. Available from: doi: 10.1016/j.ijsolstr.2014.04.002.
- Sherman, D. R. (1976) Tests of circular steel tubes in bending. *Journal of the Structural Division*. ASCE 102 (11), 2181-2195. Available from: doi: 10.1061/JSDEAG.0004478.
- Sherman, D. R. & Glass, A. M. (1974) Ultimate bending capacity of circular tubes. *Proceedings of the Annual Offshore Technology Conference*. 1974-May, 901-905. Available from: doi: 10.4043/2119-ms.
- Taras, A., Greiner, R. & Unterweger, H. (2013) *Proposal for Amended Rules for Member Buckling and Semi-compact Cross-Section Design*. Institute of Steel Structures, Graz University of Technology.
- Timoshenko, S. & Woinowsky-Krieger, S. (1959) *Theory of plates and shells*. 2nd edition. New York, McGraw-Hill.
- Walport, F., Gardner, L. & Nethercot, D. A. (2020) Equivalent bow imperfections for use in design by second order inelastic analysis. *Structures*. 26, 670-685. Available from: doi: 10.1016/j.istruc.2020.03.065.
- Walport, F., Gardner, L. & Nethercot, D. A. (2021) Design of structural stainless steel members by second order inelastic analysis with CSM strain limits. *Thin-Walled Structures*. 159, 107267. Available from: doi: 10.1016/j.tws.2020.107267.
- Wardenier, J. (2002) *Hollow sections in structural applications*. Rotterdam, Bouwen met Staal.
- Yun, X. & Gardner, L. (2018) The continuous strength method for the design of cold-formed steel non-slender tubular cross-sections. *Engineering Structures*. 175, 549-564. Available from: doi: 10.1016/j.engstruct.2018.08.070.
- Yun, X. & Gardner, L. (2017) Stress-strain curves for hot-rolled steels. *Journal of Constructional Steel Research*. 133, 36-46. Available from: doi: 10.1016/j.jcsr.2017.01.024.